Optimizing Interface Conductivity in Electronics

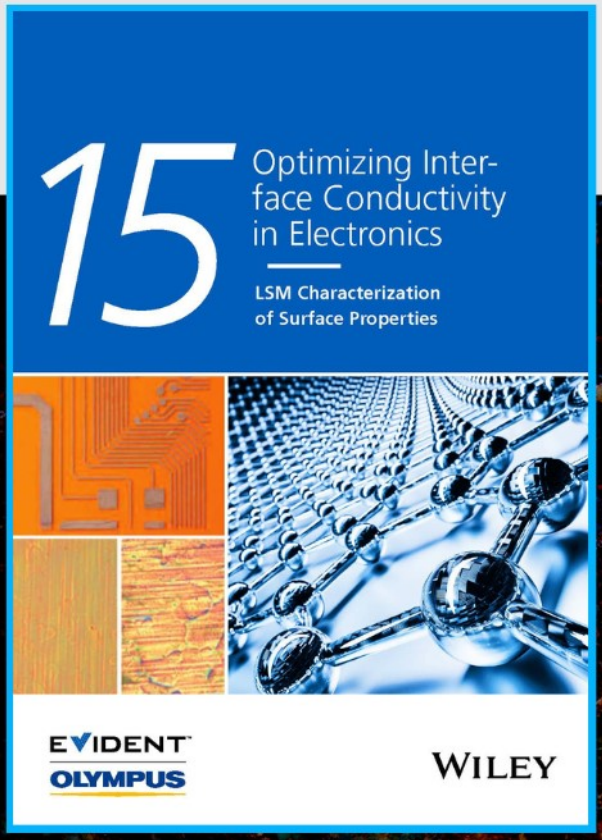

The latest eBook from Advanced Optical Metrology. Download for free.

Surface roughness is a key parameter for judging the performance of a given material's surface quality for its electronic application. A powerful tool to measure surface roughness is 3D laser scanning confocal microscopy (LSM), which will allow you to assess roughness and compare production and finishing methods, and improve these methods based on mathematical models.

Focus on creating high-conductivity electronic devices with minimal power loss using laser scanning microscopy is an effective tool to discern a variety of roughness parameters.

EVIDENT
OLYMPUS

WILEY

Check for updates

ADVANCED FUNCTIONAL MATERIALS
www.afm-journal.de

Super-Stretchable, Anti-Freezing, Anti-Drying Organogel Ionic Conductor for Multi-Mode Flexible Electronics

Yong Long, Bing Jiang, Tianci Huang, Yuxiu Liu, Jianan Niu, Zhong Lin Wang, and Weiguo Hu**

Due to their intrinsic flexibility, tunable conductivity, multiple stimulus-response, and self-healing ability, ionic conductive hydrogels have drawn significant attention in flexible/wearable electronics. However, challenges remain because traditional hydrogels inevitably faced the problems of losing flexibility and conductivity because of the inner water loss when exposed to the ambient environment. Besides, the water inside the hydrogel will freeze at the water icing temperatures, making the device hard and fragile. As a promising alternative, organogels have attracted wide attention because they can, to some extent, overcome the above drawbacks. Herein, a kind of organogel ionic conductor (MOIC) by a self-polymerization reaction is involved, which is super stretchable, anti-drying, and anti-freezing. Meanwhile, it can still maintain high mechanical stability after alternately loading/unloading at the strain of 600% for 600 s (1800 cycles). Using this MOIC, high-performance triboelectric nanogenerator (TENG) is constructed (MOIC-TENG) to harvest small mechanical energy even the MOIC electrode underwent an extremely low temperature. In addition, multifunctional flexible/wearable sensors (strain sensor, piezoresistive sensor, and tactile sensor) are realized to monitor human motions in real time, and recognize different materials by triboelectric effect. This study demonstrates a promising candidate material for flexible/wearable electronics such as electronic skin, flexible sensors, and human-machine interfaces.

1. Introduction

With the emergence and rapid rise of the Internet of Things (IoT), flexible and wearable electronics have attracted significant research attention[1–9] To satisfactorily meet the requirements of flexible electronics such as human skin, artificial muscle, and flexible sensors, device materials are expected to be stretchable,mechanically robust, and electrically conductive. Besides, as extreme conditions frequently occur in practical environments, for example, low temperature and dry weather, the device materials should also be anti-freezing, anti-drying, and thermal stable to better adapt the practical applications, and ensure the normal work for a long time [10–19] As one of promising ionic conductive flexible materials, hydrogels are widely studied because of their merits of being transparent, stretchable, and ionic conductive[10,20–29] Nevertheless, due to the limited choice of gelators[13,20,30] hydrogels have deficiencies of poor affinity to hydrophobic substances [30–32] and poor structural/environmental stability[7,13,33] Because of the free water molecules inside, most hydrogels can easily be frozen at a low temperature below zero[10–11,14–15,17] In addition, hydrogels can hardly prevent the inner water from evaporating in a dry environment, which directly leads to the loss of flexibility and electrical conductivity, and finally severely limits the applications in flexible electronics. Therefore, it is urgent to explore more suitable materials for flexible/wearable electronics[8,20,34]

As an alternative, organogel can easily overcome the above problems because the solvents available for preparing organogels are much broader than those for hydrogels, which provides more applications than hydrogels[9,13,35–45] In this work, we designed a stretchable and multifunctional organogel ionic conductor (MOIC) via a facile self-polymerization reaction in a glycol-water binary solvent. This organogel was conductive, flexible, water-retaining, anti-freezing, and thermally stable. It

Y. Long, Y. Liu, J. Niu, Z. L. Wang, W. Hu
CAS Center for Excellence in Nanoscience
Beijing Key Laboratory of Micro-nano Energy and Sensor
Beijing Institute of Nanoenergy and Nanosystems
Chinese Academy of Sciences Beijing
Beijing 101400, P. R. China
E-mail: zhong.wang@mse.gatech.edu; huweiguo@binn.cas.cn

The ORCID identification number(s) for the author(s) of this article can be found under https://doi.org/10.1002/adfm.202304625

DOI: 10.1002/adfm.202304625

B. Jiang, T. Huang, Z. L. Wang, W. Hu
Center on Nanoenergy Research
School of Physical Science and Technology
Guangxi University
Nanning 530004, P. R. China

Y. Liu, J. Niu, Z. L. Wang, W. Hu
School of Nanoscience and Technology
University of Chinese Academy of Sciences
Beijing 100049, China

Z. L. Wang
School of Materials Science and Engineering
Georgia Institute of Technology
Atlanta GA 30332-0245, USA

 © 2023 Wiley-VCH GmbH

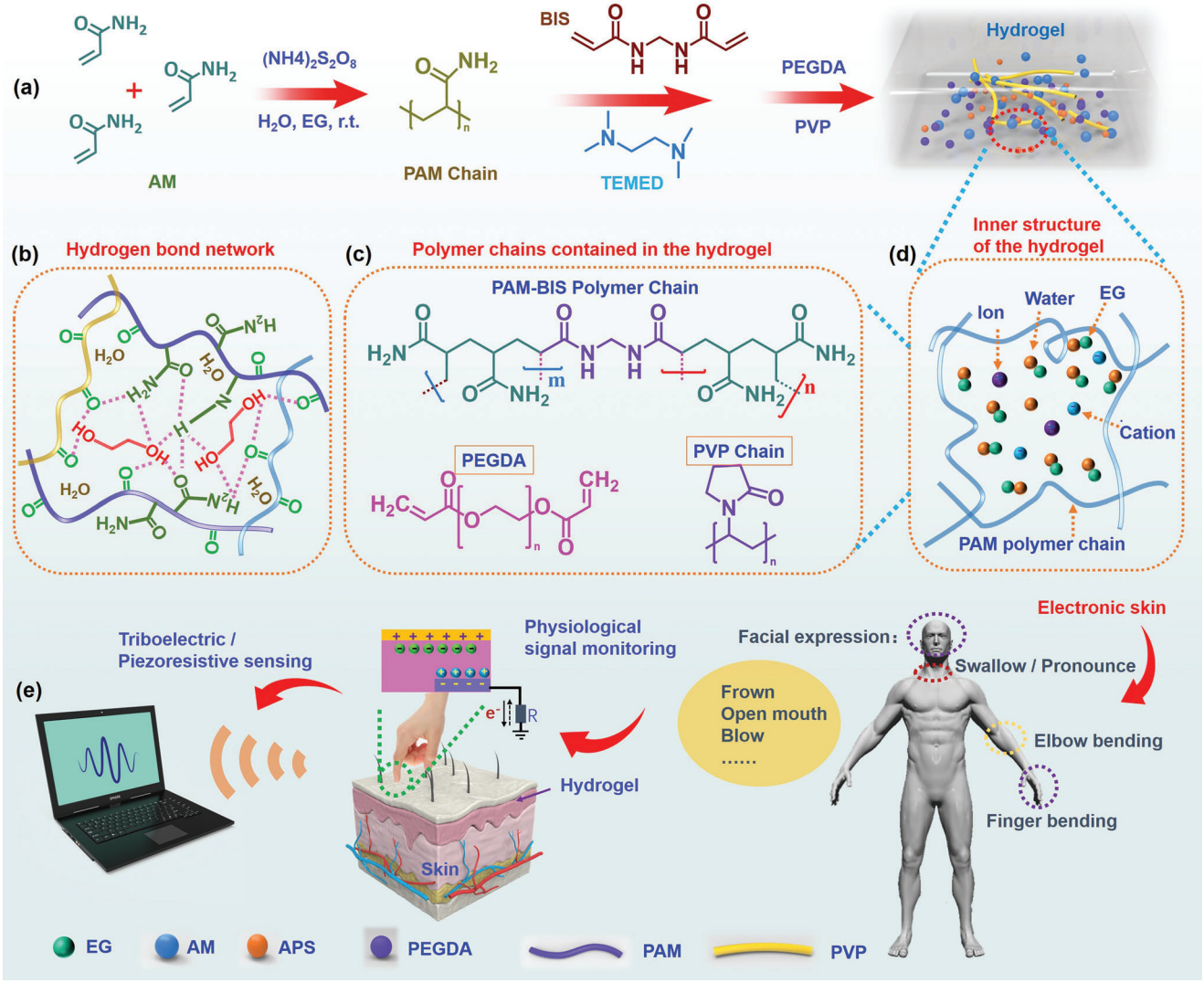

Figure 1. The preparation process of the MOIC and its application diagram. a) The preparation process and its reaction principle of the MOIC. b) Hydrogen bond network between the polymer chains framework inside the MOIC. c) The molecular structures of the main polymer chains consisting the MOIC, including PAM-BIS polymer chains, the PVP chains, and the PEGDA chains. d) The inner structure of the MOIC, including polymer chains framework, ions, a large number of free water molecules-EG clusters. e) The strain sensor and the triboelectric sensor applications of the MOIC in flexible/wearable electronics.

exhibits super strain (as high as 9000%), antifreeze (as low as −30 °C), and excellent water loss resistance. It can still maintain high mechanical stability after alternately loading/unloading at the strain of 600% for 600s (1800 cycles). With the obtained MOIC, a flexible and wearable multifunctional sensor was constructed to detect small human movements. Besides, a high-performance TENG was assembled with the obtained MOIC. By detecting the voltage of the triboelectricity after contact/separation with different material surfaces, a tactile sensor was realized to recognize different materials. The MOIC shows promising applications in TENG for small energy harvest, and strain/tactile sensors for small human motion monitoring.

2. Results and Discussion

As described in the Experimental Section, the conductive and stretchable MOIC was obtained via a facile self-polymerization reaction at room temperature. Generally, acrylamide (AM) monomer and PVP were first dissolved in the binary mixed solvent of H_2O/ethylene glycol (EG) under continuous magnetic stirring at room temperature. Then, polyethylene glycol (575) (PEGDA575) and NaCl solution followed into the above-mixed solution, and kept stirring for 5 h (**Figure 1**a), where the volume ratio of EG and water is 3:1. After the above-mixed solution dispersed homogeneously, a certain amount of ammonium persulfate (APS) initiator, and *N*,*N*′-methylene bisacrylamide

© 2023 Wiley-VCH GmbH

16163028, 0, Downloaded from https://onlinelibrary.wiley.com/doi/10.1002/adfm.202304625 by Georgia Institute Of Technology, Wiley Online Library on [06/08/2023]. See the Terms and Conditions (https://onlinelibrary.wiley.com/terms-and-conditions) on Wiley Online Library for rules of use; OA articles are governed by the applicable Creative Commons License

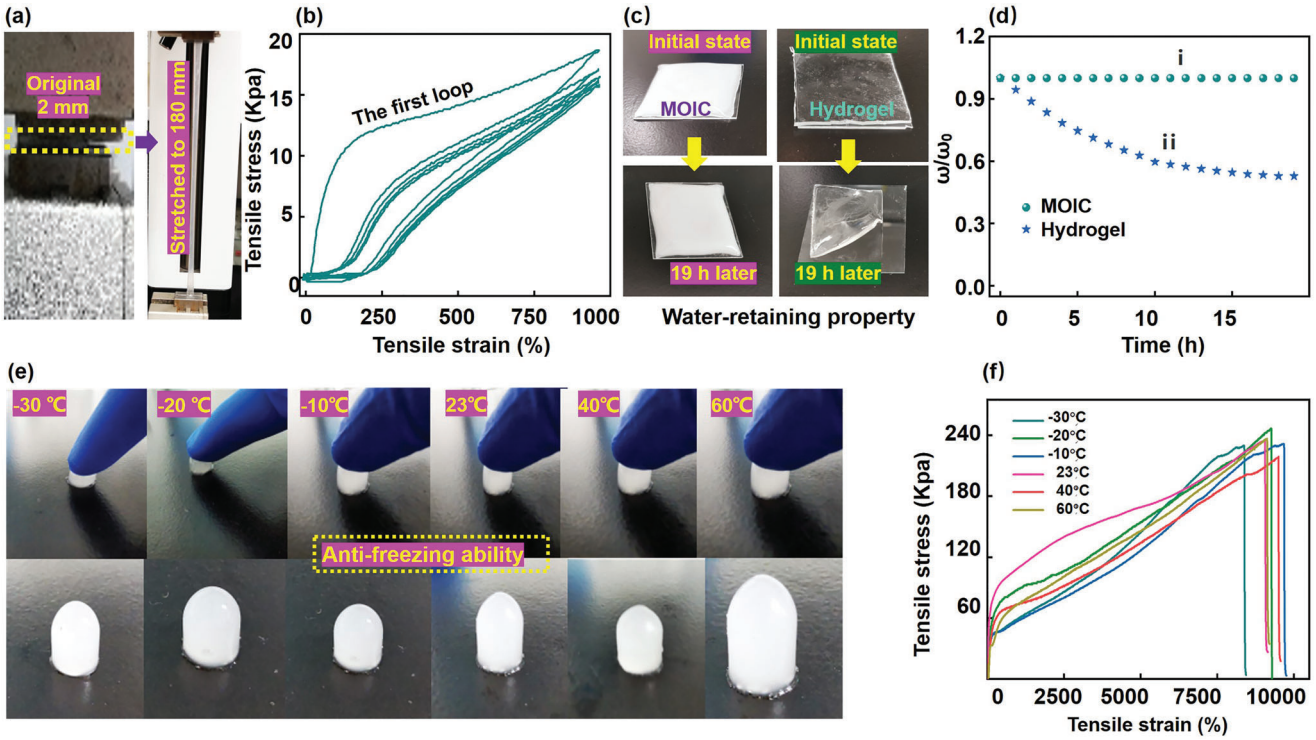

Figure 2. The basic characterizations of the MOIC. a) The photo of the tensile test of the MOIC, stretching from its original length of 2 to 180 cm. b) Tensile stress–strain curves of the MOIC during five consecutive loading-unloading cycles at a strain of 965%. c) The visual morphology of the anti-drying property of the MOIC compared with ordinary hydrogel before and after being dried for 19 h. d) The relative weight changes of the MOIC in the air at room temperature, compared with the ordinary hydrogel. e) The anti-freezing property of the MOIC shows that when pressed under different temperature ranges (from −30 to 60 °C), the MOIC still exhibited good flexibility. d) Tensile stress–tension strain curves of the MOIC from the temperature range of −30 to 60 °C.

(BIS) chemical cross-linker were followed in sequence. Finally, *N*,*N*,*N*′,*N*′-tetramethylethylenediamine (TEMED) catalyst was quickly injected into the reaction mixture system to accelerate the self-polymerization reaction. After the TEMED was added, the precursor solution of the MOIC was quickly poured into a glass culture dish. All the reactants are shown in Figure 1a. The solidification process of the precursor solution was completed with the self-polymerization reaction proceeding vigorously in about 30 minutes, and finally, the MOIC was obtained.

During the formation process of the MOIC, both non-covalent bonds and covalent bonds formed and coexisted.[36] On the one hand, abundant oxygen-containing groups (hydroxy, carbonyl, acylamino) on the polymer chains crosslinked with each other via hydrogen bonds, forming hydrogen bond networks (non-covalent bond networks), as exhibited in Figure 1b. The molecular structures of the three main polymer chains consisting of the MOIC are shown in Figure 1c, including the PAM-BIS polymer chains, the PVP chains, and the PEGDA chains. On the other hand, PAM polymer chains were generated during the self-polymerization of AM molecules by covalent bond, and then the formed PAM polymer chains crosslinked with the BIS molecules also via covalent bond. Besides, a third interaction, electrostatic attraction, also existed between ions (Na^+, NH_4^+) and the lone pair electrons on the oxygen atom of the carbonyl. Additionally, a large number of H_2O-EG clusters existed in the form of intermolecular hydrogen bonding, Figure 1d. These forces significantly improved the flexibility and mechanical strength of the resultant MOIC. The obtained MOIC was applied as a strain sensor to monitor various kinds of human motions and as a tactile sensor to recognize different materials via the triboelectric effect, as shown in Figure 1e.

2.1. Super Stretchability, Anti-Drying Ability, Water Retention, Anti-Freezing Ability, and Thermal Stability

The basic properties of the as-prepared MOIC, including stretchability, anti-freezing, and anti-drying abilities, were studied, respectively, and the corresponding characterizations are shown in **Figure 2**. The excellent stretchability of the MOIC is visually exhibited in Figure 2a that it can be stretched from its original length of 2 mm to as long as 180 mm, also the stress–strain curve in Figure S1 (Supporting Information) showed that the MOIC can be stretched to 9000% of its original length at room temperature. It could recover to its original state quickly after being stretched (Figure S2, Supporting Information). As was discussed above, since we have introduced both covalent bonds and non-covalent bonds in the MOIC structure, the covalent bond (the first network, mainly from the formation of the PAM chain) played the role of dissipating energy during the stretching process. The entanglement of polymer chain networks produced a second network by hydrogen bonds, the non-covalent bond,

© 2023 Wiley-VCH GmbH

16163028, 0, Downloaded from https://onlinelibrary.wiley.com/doi/10.1002/adfm.202304625 by Georgia Institute Of Technology, Wiley Online Library on [06/08/2023]. See the Terms and Conditions (https://onlinelibrary.wiley.com/terms-and-conditions) on Wiley Online Library for rules of use; OA articles are governed by the applicable Creative Commons License

endowing the MOIC an extremely stretchability (9000%). To further understand and demonstrate the mechanism of the MOIC's high stretchability, we measured the continuous loading-unloading cycle curve with the tensile strain of 965% (Figure 2b). The tensile stress – tensile strain curve in Figure 2b gave a quantitative and accurate measurement of its stretchability. From the curves, we can observe a clear hysteresis in the first loop, which no longer appeared in the rest of the load-unload cycle curves, indicating that the covalent bond crosslinked networks in the first cycle were broken, releasing the internal energy. In the rest of the loading-unloading curves, the MOIC exhibited slight hysteresis, and no obvious deformation was observed, implying the existence of reversible non-covalent bonds (the hydrogen bond networks which were formed by the entanglement of the different polymer chains).

Therefore, based on the discussion above, the ultimate super stretchability of the MOIC could be explained as follows. When the MOIC was stretched, the first network from the covalently cross-linked bond acted as a sacrificial bond, which released the internal stress during its broken process, and greatly dissipated the internal energy. At the same time, the second network, the non-covalently cross-linked bond, was entangled with the broken PAM fragments. The free hydrogen bonds between the entangled polymer chains and chain fragments were in dynamic rupture and reorganization, thereby achieving the super stretchability of the MOIC.

To further study the environmental suitability of the MOIC, the anti-drying ability was then studied by placing a piece of MOIC slice directly in the air at room temperature for as long as 19 hours, and the corresponding weight changes (ω/ω_0) every hour were recorded. Meanwhile, as a comparison, the weight of an ordinary hydrogel piece (with pure water as the reaction solution) was also monitored and measured under the same environmental conditions. As shown in Figure 2c, over the whole monitoring period, the morphology of the MOIC showed no change, while the hydrogel became hard due to its inner water loss. Furthermore, from the ω/ω_0–Time curves in Figure 2d, the weight of the MOIC showed a little decrease (Figure 2d-i), demonstrating its excellent anti-drying ability and water-retaining properties. However, as a sharp contrast, the ω/ω_0 of the hydrogel gave an obvious decrease, even fell to half of its original weight in 19 h (Figure 2d-ii), which means that the ordinary hydrogel lost water seriously when exposed to the air in room temperature. This control experiment exhibited the excellent anti-drying ability and water retention properties of the prepared MOIC.

In recent years, due to the frequent occurrence of extreme weather (extreme cold or extremely hot). For flexible/wearable electronics, exposure to extreme environments during the work process is inevitable. Consequently, the structural stability of the device materials in an extremely cold or hot environment is another crucial factor in determining the stable work of a device. Therefore, the elasticity and the stretchability of the MOIC in a wide temperature range were carefully considered. Specifically, in a wide temperature range of −30 to 60 °C, six temperature points were selected (−30, −20, −10, 23, 40, and 60 °C). The as-prepared MOIC was stored at these selected temperature points for several hours and then pressed heavily from its original cylindrical shape to nearly its bottom circular shape. When the external pressure was removed, all the MOIC samples immediately restored to their original shape, as shown in Figure 2e. Besides, for these different temperature-treated MOIC samples, the stretchability of every sample was also tested, and the corresponding Tensile strain–Tensile stress curves are shown in Figure 2f, from which we can observe that all the curves were close to each other. These results exhibited the good elasticity, stretchability, and flexibility of the MOIC under different temperature ranges (from −30 to 60 °C) and indicated that the MOIC had an excellent anti-freezing ability and thermal stability. The anti-freezing property is attributed to the introduced EG molecules which disrupt the hydrogen bonds between H_2O molecules. After mixing with H_2O molecules, the EG molecules can form molecular clusters with H_2O molecules, therefore the saturated vapor pressure of original water is significantly reduced, leading to the freezing point decrease.

2.2. Applications in TENGs and Tactile Sensors

According to the basic characterizations and discussions above, the as-prepared MOIC demonstrated the advantages of super stretchability, anti-drying ability, water retention, anti-freezing ability, and thermal stability. These merits are ideal for energy-harvesting devices and flexible/wearable electronics. Therefore, we constructed a contact/separating mode TENG (MOIC-TENG) using the as-prepared MOIC as the TENG's electrode (**Figure 3**).

For the MOIC-TENG, a single-mode sandwiched structure was adopted. Specifically, a MOIC slice was placed on a piece of acrylic plate, and then on the surface of the MOIC was covered with a polytetrafluoroethylene (PTFE) film, which, due to its strong electronegativity, served as one of the electrification layers (a piece of butyronitrile film acted as the other electrification layer that was fixed on the linear motor's surface). The MOIC electrode was connected by a commercial copper wire to an external Keithley electrometer 6514 to detect and record the electrical output performances of the MOIC-TENG. The MOIC-TENG was driven by a linear motor. The working mechanism of the single-mode MOIC-TENG is schematically shown in Figure 3a, at the initial stage (step 1), when the butyronitrile film was driven by a linear motor to contact with the PTFE film of the MOIC-TENG completely (with the contact area of 2.5 cm × 2.5 cm), due to the triboelectric effect, triboelectric charges are generated on the interfaces of the two electrification layers. At this very moment, the same amount of opposite charges was induced on the back side. Then, with the gradual separating process of the two electrification layer surfaces, the charges on the PTFE film could not be entirely offset by the opposite charges on the butyronitrile surface (step 2 in Figure 3a). Therefore, the superfluous charges on the PTFE surface would attract negative ions in the MOIC. These attracted ions began accumulating on the PTFE's backside surface, which was contacted with the MOIC directly. With the two electrification layers moving against each other, a potential difference between the two surfaces will be generated, which drives the electrons to flow from the external circuit to the MOIC. By this means, the positive ions in the MOIC migrated to accumulate at the surface of the MOIC (step 3 in Figure 3a). The resulting open circuit voltage (V_{OC}) was detected to be as high as 160 V (Figure 3b). The corresponding short-circuit current (I_{SC}) and the short circuit condition (Q_{SC}) were detected to be ≈7 μa (Figure S3,

© 2023 Wiley-VCH GmbH

16163028, 0, Downloaded from https://onlinelibrary.wiley.com/doi/10.1002/adfm.202304625 by Georgia Institute Of Technology, Wiley Online Library on [06/08/2023]. See the Terms and Conditions (https://onlinelibrary.wiley.com/terms-and-conditions) on Wiley Online Library for rules of use; OA articles are governed by the applicable Creative Commons License

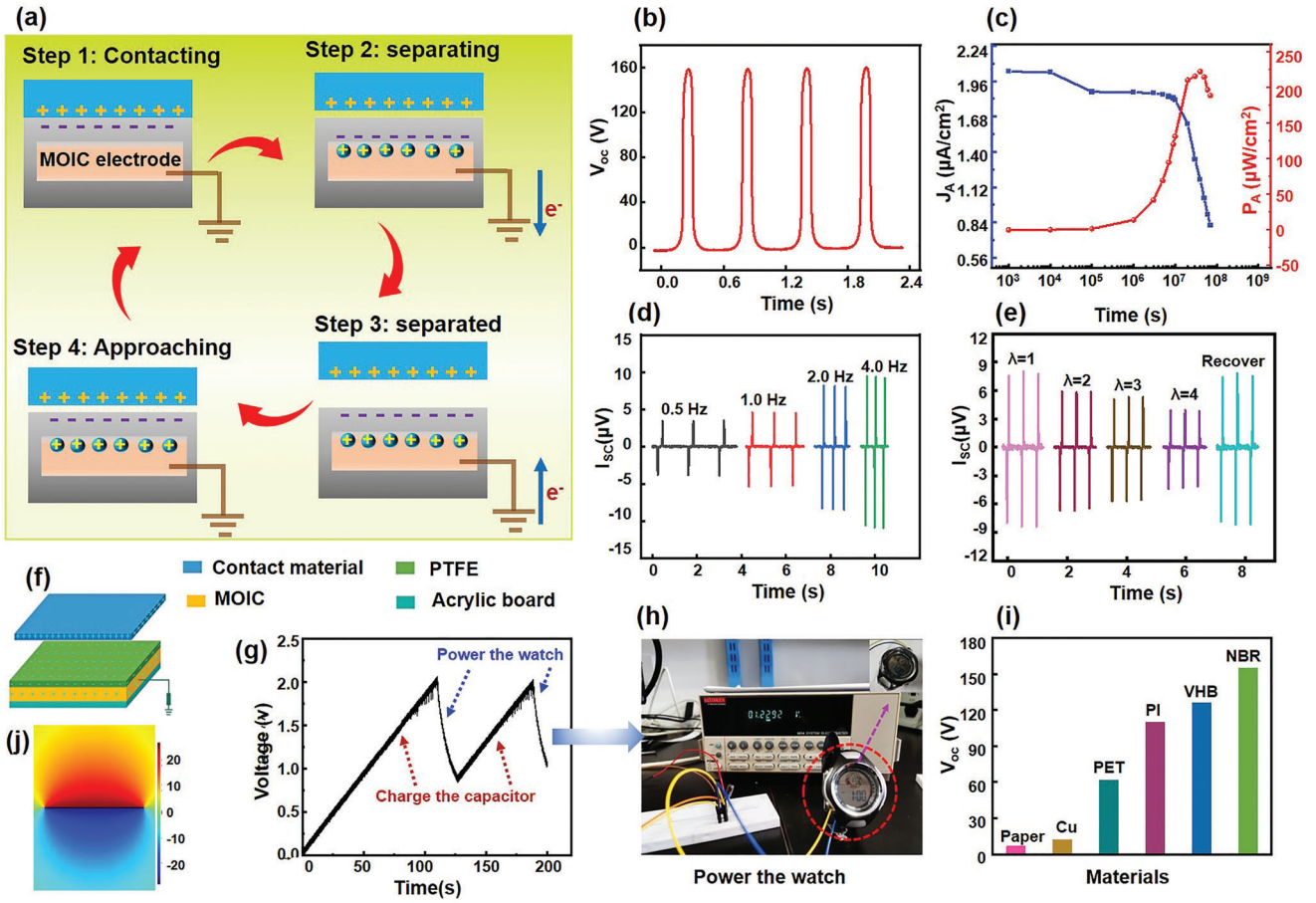

Figure 3. The electric performance of the MOIC-TENG and its applications. a) The working principle of the MOIC-TENG includes four contact/separating stages. b) Open-circuit voltage (*Voc*) of the MOIC-TENG at 2.0 Hz. c) Current density (J_A) and power density (P_A) of the MOIC-TENG with the external load resistance. d) Short-circuit current (I_{SC}) output at different frequencies. e) I_{SC} under different tensile strains. f) The construction of the MOIC-TENG. g) The voltage distribution when charging a capacitor of 2.2 μF by the MOIC-TENG to power commercial electronic watches (at this time the MOIC-TENG's electrode was pretreated at −20 °C for 12 h). h) The optical photographs of powering the commercial electronic watches. i) Peak *Voc* values of self-powered MOIC-TENG to recognize six different materials. j) Fitting the surface charge distribution when separating nitrile and PTFE with Comsol 5.2.

Supporting Information) and ≈60 nC (Figure S4, Supporting Information). The maximum power density of MOIC-TENG was calculated to be 225 μw cm^{-2} (4), and the maximum current density was ≈1.98 μA cm^{-2} by changing the external resistance (the matched maximum resistance is ≈100 MΩ). We also measured the current output of the MOIC-TENG at different frequencies. As shown in Figure 3d, the current values increased with the frequency and are relatively stable below 4 Hz, which means we can adjust the current output values according to the specific needs. Hence, the MOIC-TENG showed broad prospects in the field of flexible electronics.

According to the experiment results and analysis in Figure 2, the MOIC exhibited excellent stretchability and flexibility. So, the I_{SC} of the MOIC-TENG with its MOIC electrode under different tensile strains (λ) was measured. From Figure 3e, we can observe that when the MOIC electrode was in unstretched state ($\lambda = 1$), the MOIC-TENG gave the highest I_{SC} value. However, as the λ became larger, the corresponding I_{SC} value became smaller ($\lambda =$ 2, 3, 4). When the MOIC electrode recovered to its original state ($\lambda = 1$), the corresponding I_{SC} value also recovered. The possible reason is that MOIC was stretched, its thickness decreased, leading to the cross-sectional area (CSA) reduction, and at the same time, the length of the MOIC increased. Finally, the resistance value of the electrode increased (according to the formula: $R = \rho \cdot L/S$, where R is the resistance, ρ is the density of the electrode material, L represents the electrode length, and S is the cross-sectional area of the electrode material). This result indicated the excellent flexibility of the MOIC, and it can ensure stable output performances of the electronic device when recovered from stretch or deformation.

The configuration of the sandwiched MOIC-TENG is shown in Figure 3f. It was demonstrated that this MOIC-TENG could effectively harvest mechanical energy and drive small commercial electronics. Here, firstly a capacitor of 2.2 μF was charged within 110 s at a frequency of 2 Hz (Figure 3g), and then a commercial electronic watch was powered successfully within 16 s (Figure 3h). Besides, the MOIC-TENG can also light up small commercial lights. As shown in (Figure S5, Supporting

© 2023 Wiley-VCH GmbH

16163028, 0, Downloaded from https://onlinelibrary.wiley.com/doi/10.1002/adfm.202304625 by Georgia Institute Of Technology, Wiley Online Library on [06/08/2023]. See the Terms and Conditions (https://onlinelibrary.wiley.com/terms-and-conditions) on Wiley Online Library for rules of use; OA articles are governed by the applicable Creative Commons License

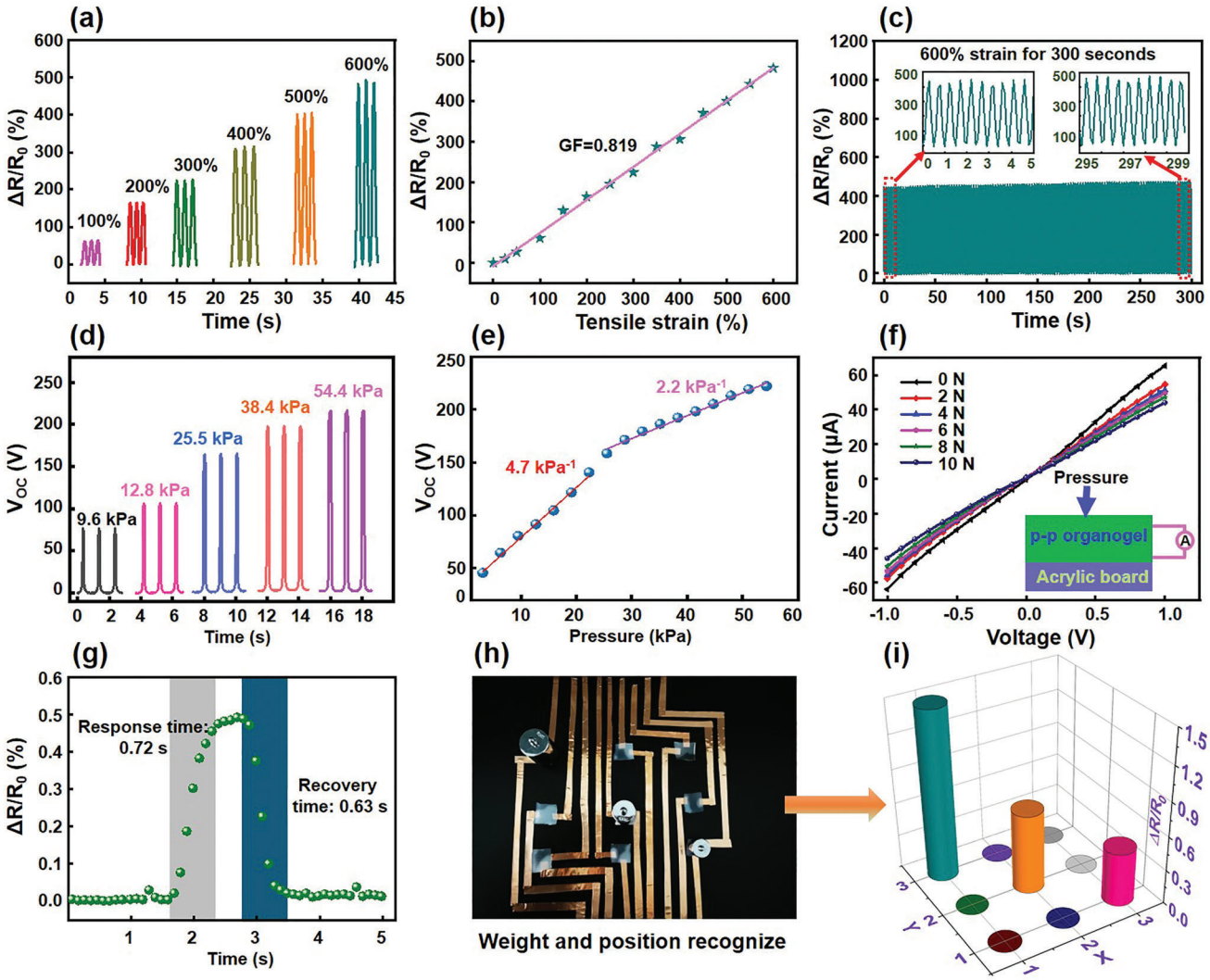

Figure 4. Characterization and application of strain/piezoresistive sensors of the MOIC. a) Relative resistance change from the tensile strains of 100% to 600%. b) The measurement gauge factor of the MOIC strain sensor. c) Output stability test of the MOIC strain sensor under 600 cycles (300 s) with a tensile strain of 600%. d) Response to different pressure when the MOIC was used as a piezoresistive sensor. e) Sensitivity measurement of the MOIC piezoresistive sensor. f) The linear relation of the *I–V* curves with small forces. g) Fast responsive and recovery time of the MOIC piezoresistive sensor. h) Image of the sensor matrix with 3 pixels × 3 pixels. i) The corresponding voltage signal response of the sensor matrix.

Information), with the same MOIC-TENG and frequency, 26 red commercial light-emitting diodes (LEDs) are successfully lit up. It's worth noting that the MOIC-TENG electrode used in Figure 3g,h was pretreated at −20 °C for 12 h, indicating that this MOIC-TENG can still work normally and stably even the TENG's electrode underwent an extremely low temperature.

More importantly, using our MOIC, a tactile sensor was realized to identify different materials. When the MOIC sensor was in contact with a certain kind of material, the electrical signal would be generated because of the contact electrification effect. When contacting different materials, a unique electrical signal would be generated. By detecting this electrical signal, a special kind material could be recognized. To demonstrate this application, we first selected four different materials with their surfaces as flat as possible, including copper (Cu), polyethylene glycol terephthalate (PET), polyimide (PI), and nitrile rubber (NBR). Then we fixed these four materials to the linear motor, respectively, and used the same force to drive every kind of these materials to contact with the MOIC sensor. Figure 3i shows the electrical response signals (V_{OC}) generated by contacting with every material. Finally, the surface charge distribution when separating nitrile with PTFE was fitted with Comsol 5.2 (Figure 3j).

2.3. Applications in Strain/Piezoresistive Sensors

The MOIC can also exhibit strain/piezoresistive sensing performances and could be used as wearable strain sensors and e-skins. Here, we measured the relative resistance changes ($\Delta R/R0$) of the MOIC against the different tensile strains (**Figure 4**a). Obviously, in a wide tensile strain range, from 100% to 600%, the corresponding $\Delta R/R_0$ values were not only quite distinguishable,

© 2023 Wiley-VCH GmbH

16163028, 0, Downloaded from https://onlinelibrary.wiley.com/doi/10.1002/adfm.202304625 by Georgia Institute Of Technology, Wiley Online Library on [06/08/2023]. See the Terms and Conditions (https://onlinelibrary.wiley.com/terms-and-conditions) on Wiley Online Library for rules of use; OA articles are governed by the applicable Creative Commons License

16163028, 0, Downloaded from https://onlinelibrary.wiley.com/doi/10.1002/adfm.202304625 by Georgia Institute Of Technology, Wiley Online Library on [06/08/2023]. See the Terms and Conditions (https://onlinelibrary.wiley.com/terms-and-conditions) on Wiley Online Library for rules of use; OA articles are governed by the applicable Creative Commons License

but also increased monotonously with the corresponding tensile strain increase, indicating that the MOIC strain sensor could be used in a wide detectable tensile strain range. According to Figure 4a, the Gauge Factor (GF, defined as $GF = (\Delta R/R_0)/\lambda$) could be calculated to be 0.819 in the full tested tensile strain range (figure 4b). In addition, the long-term stability of the $\Delta R/R_0$ was researched. As was shown in Figure 4c, under the tensile strain of 600%, 600 continuous stretching repetitions (300 s) were performed, and the corresponding $\Delta R/R_0$ response curves were relatively stable with no noticeable fluctuation. Besides, $\Delta R/R_0$ stabilities under every tensile stain (100%, 200%, 300%, 400%, 500%, 600%) were also studied, and their corresponding strain response curves were shown in Figures S6–S10 (Supporting Information). Except for the situations of tensile strain, this kind of MOIC also showed obvious responses to different external pressure. First, large pressures, from the pressure range of 9.6 to 54.4 kPa, were respectively applied to the MOIC piezoresistive sensor. As exhibited in Figure 4d, five different pressures were tested (9.6, 12.8, 25.5, 38.4, and 54.4 kPa), and the corresponding electrical signal response (V_{OC}) showed a steady increase with the pressure increasing. According to the pressure response results in Figure 4d, the corresponding sensitivity of the piezoresistive sensor could be calculated. Of the two linear ranges, the sensitivities were respectively calculated to be 4.7 and 2.2 kPa^{-1}. Also, we found that the MOIC piezoresistive sensor can respond to even extremely small forces. As exhibited in Figure 4f, a series of small forces (0, 2, 4, 6, 8, and 10 N), the corresponding *I*–*V* curves under different pressures were linear and distinguishable, showing the high sensitivity of the MOIC piezoresistive sensor. By loading–unloading an external pressure, the response time and recovery time of the MOIC piezoresistive sensor are detected to be 0.72 and 0.63 s, respectively (Figure 4g).

To further investigate the piezoresistive sensing application of the MOIC, a piezoresistive sensor array with 9-pixel pressure units was assembled (Figure 4h). In this sensor array, every MOIC square served as a discrete sensor unit. Once an external pressure was applied on the surface of a sensor unit, the corresponding electric response signals ($\Delta R/R_0$) were detected and recorded in real time. The contact position and the pressure could be displayed vividly in a 3D mapping diagram (Figure 4i). For example, we put weights of 200, 100, and 50 g into three different pixels (Figure 4i), the corresponding positions were displayed, and the different heights of the column represented the different weights. The results indicated that the sensor array assembled from the MOIC could be used to recognize both the pressure position and the pressure in real-time.

To further evaluate the sensing performances of the MOIC in wearable electronics, we used the as-prepared MOIC (pretreated at −20 °C for 12 h) as electronic skin to monitor various human movements (**Figure 5**). Specifically, the pretreated MOIC film was attached to the corresponding position of the human body, and connected to an electrochemical workstation. When the monitored position of the human body moved, the corresponding electrical signal could be reflexed by the MOIC electronic skin sensor and be detected. By this means, we have successfully realized the recognition of cheek moving (Figure 5a), different degrees of frowning (Figure 5b), swallowing (Figure 5c), mouth blowing (Figure 5d), elbow bending (Figure 5e), finger pressing (Figure 5f), different degree of finger bending (Figure 5g). Besides, even water drops could be detected (Figure 5h). The results indicated that the as-prepared MOIC could serve as a promising candidate material for the applications of flexible/wearable devices, e-skins, and human-machine interfaces based on its strain/piezoresistive sensing properties even the MOIC underwent an extremely low temperature.

3. Conclusion

In summary, a multifunctional organogel ionic conductor (MOIC) was prepared by a facile self-polymerization reaction in a glycol–water binary solvent. The MOIC was demonstrated to be super stretchable (stretched to as high as 9000%), antifreezing (as low as −30 °C), anti-drying (−30 to 60 °C), water-retaining, and thermal stable. Meanwhile, it can still maintain high mechanical stability after alternately loading/unloading at the strain of 600% for 600 s (1800 cycles). Using this MOIC, high-performance triboelectric nanogenerator (TENG) was constructed (MOIC-TENG) to harvest small mechanical energy, and drive small commercial electronics even the MOIC electrode underwent an extremely low temperature. In addition, multifunctional flexible and wearable sensors were realized, including strain sensor, piezoresistive sensor, and tactile sensor. The strain/piezoresistive sensors were used to monitor various human motions in real-time (cheek moving, different degrees of frowning, swallowing, mouth blowing, elbow bending, finger pressing, different degrees of finger bending, and even water drops falling). And the tactile sensor can recognize different materials by the triboelectric effect. This work demonstrates a promising candidate material for flexible/wearable electronics such as electronic skin, flexible sensors, and human-machine interfaces.

4. Experimental Section

Materials: Acrylamide (AM), ammonium persulfate (APS), ethylene glycol (EG), and poly(ethylene glycol) diacrylate (PEGDA 575) were purchased from Shanghai Macklin Biochemical Co., Ltd. Tetramethylethylenediamine (TEMED) was purchased from Aladdin. Sodium chloride (NaCl) was purchased from TIANJIN FUCHEN. All the reagents were analytical reagents.

Preparation of the MOIC: The as-obtained MOIC was synthesized by a self-polymerization reaction using acrylamide (AM) and Polyvinylpyrrolidone (PVP) as double networks, with poly(ethylene glycol) diacrylate (PEGDA) as the crosslinker, the ammonium persulfate (APS) served as the initiator of the polymerization reaction, and tetramethylethylenediamine (TMEDA) acting as the catalyst. Specifically, 10.0 g AM and 1.0 g PVP powder were dissolved into 15 mL EG and 5 mL NaCl solution under continuous magnetic stirring for 5 h at a rotation speed of 800 rpm at room temperature. Ten microliters of PEGDA and 1.0 g APS were added into the above solution under stirring for another 10 min. Then 0.1 µL TEMED was injected into the above reaction mixture for several seconds of stir. Subsequently, the final mixture solution was poured into a Petri dish to obtain MOIC.

Characterization and Measurement: A liner motor (LinMot E1100) was powered for the contact-separation working process of the TENG. The output signal was measured by Keithley electrometer 6514. The stress–strain curve eas tested by an ESM301/Mark-10 system. Relative resistance was tested by electrochemical workstation (CHI760E). The freezing of materials is done with a freeze-dryer. (SCIENTZ-10N).

 © 2023 Wiley-VCH GmbH

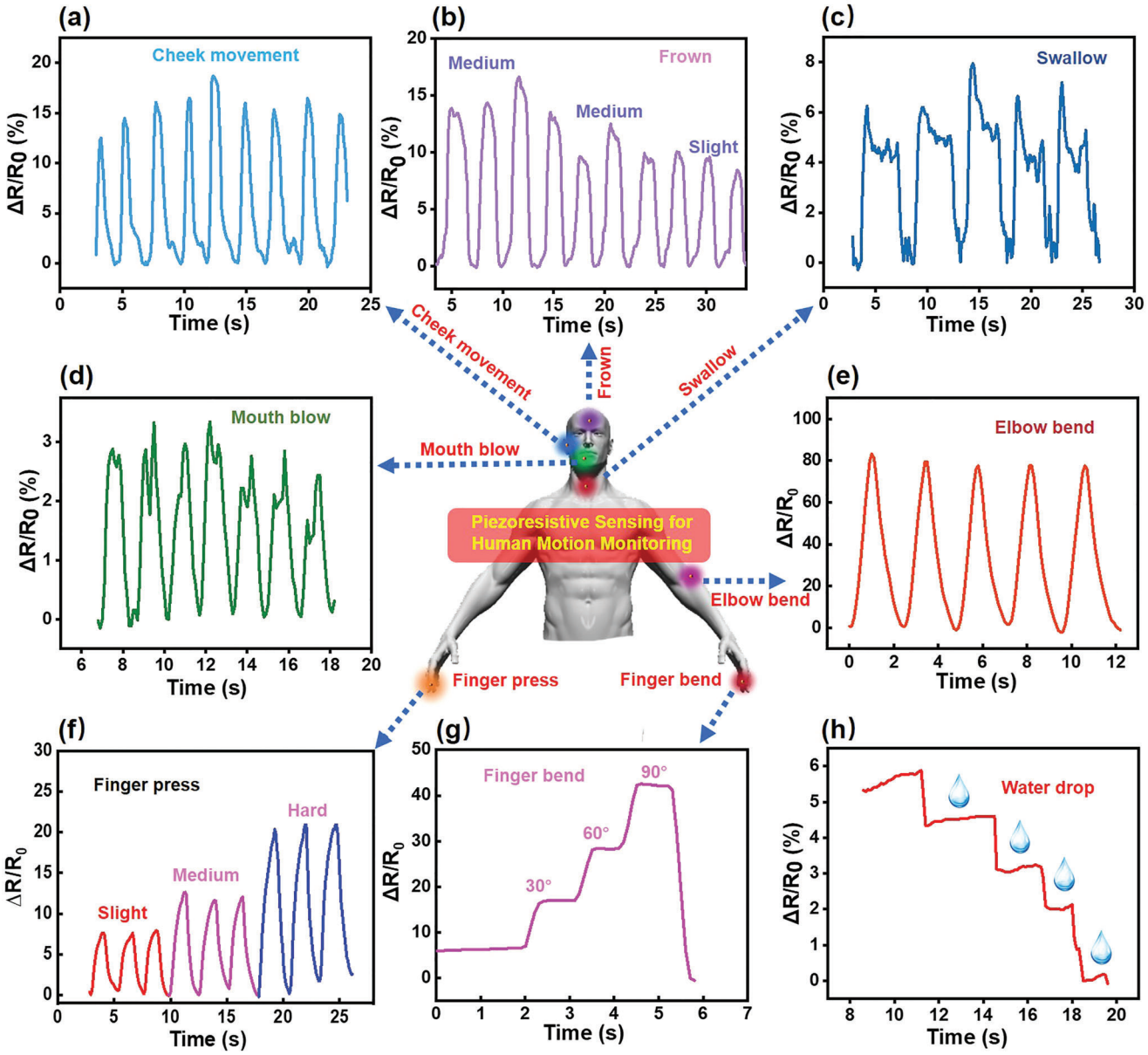

Figure 5. The strain/piezoresistive sensors to monitor various human motions in real time. a) Cheek moving. b) Frowning. c) Swallowing. d) Mouth blowing. e) Elbow bending. f) Finger pressing. g) Finger bending. h) Water drops falling.

Supporting Information

Supporting Information is available from the Wiley Online Library or from the author.

Acknowledgements

Y.L. and B.J. contributed equally to this work. The authors thank for the support from the National Key R&D Program of China (No. 2021YFA1201603) and the National Natural Science Foundation of China (Nos. 22001018, 52192610, 52173298), and the Fundamental Research Funds for the Central Universities.

Conflict of Interest

The authors declare no conflict of interest.

Data Availability Statement

The data that support the findings of this study are available from the corresponding author upon reasonable request.

Keywords

organogels, ionic conductors, piezoresistive sensors, strain sensors, triboelectric nanogenerators

© 2023 Wiley-VCH GmbH

16163028, 0, Downloaded from https://onlinelibrary.wiley.com/doi/10.1002/adfm.202304625 by Georgia Institute Of Technology, Wiley Online Library on [06/08/2023]. See the Terms and Conditions (https://onlinelibrary.wiley.com/terms-and-conditions) on Wiley Online Library for rules of use; OA articles are governed by the applicable Creative Commons License

Received: April 26, 2023
Revised: May 23, 2023
Published online:

[1] Y. Ling, T. An, L. W. Yap, B. Zhu, S. Gong, W. Cheng, *Adv. Mater.* **2020**, *32*, 1904664.
[2] H. C. Ates, P. Q. Nguyen, L. Gonzalez-Macia, E. Morales-Narváez, F. Güder, J. J. Collins, C. Dincer, *Nat. Rev. Mater.* **2022**, *7*, 887.
[3] J. Wei, P. Xiao, T. Chen, *Adv. Mater.* **2023**, *n/a*, 2211758.
[4] T. Chen, Q. F. Shi, M. L. Zhu, T. Y. Y. He, L. N. Sun, L. Yang, C. Lee, *ACS Nano* **2018**, *12*, 11561.
[5] Z. M. Lin, J. Yang, X. S. Li, Y. F. Wu, W. Wei, J. Liu, J. Chen, J. Yang, *Adv. Funct. Mater.* **2018**, 28.
[6] X. Pu, M. M. Liu, X. Y. Chen, J. M. Sun, C. H. Du, Y. Zhang, J. Y. Zhai, W. G. Hu, Z. L. Wang, *Sci. Adv.* **2017**, 3.
[7] Y. Y. Lee, H. Y. Kang, S. H. Gwon, G. M. Choi, S. M. Lim, J. Y. Sun, Y. C. Joo, *Adv. Mater.* **2016**, *28*, 1636.
[8] Y. Long, Z. Wang, F. Xu, B. Jiang, J. Xiao, J. Yang, Z. L. Wang, W. Hu, *Small* **2022**, *18*, 2203956.
[9] Y. Zhao, Y. Ohm, J. Liao, Y. Luo, H. Y. Cheng, P. Won, P. Roberts, M. R. Carneiro, M. F. Islam, J. H. Ahn, L. M. Walker, C. Majidi, *Nat. Electron.* **2023**, *6*, 206.
[10] X. Dai, Y. Long, B. Jiang, W. Guo, W. Sha, J. Wang, Z. Cong, J. Chen, B. Wang, W. Hu, *Nano Res.* **2022**, *15*, 5461.
[11] Z. Zhou, K. Liu, Z. Ban, W. Yuan, *Composites, Part A* **2022**, *154*, 106806.
[12] C. Liu, R. Zhang, Y. Wang, J. Qu, J. Huang, M. Mo, N. Qing, L. Tang, *J. Mater. Chem. A* **2023**, *11*, 2002.
[13] M. A. Kuzina, D. D. Kartsev, A. V. Stratonovich, P. A. Levkin, *Adv. Funct. Mater.* **2023**, *n/a*, 2301421.
[14] Y. Jian, S. Handschuh-Wang, J. Zhang, W. Lu, X. Zhou, T. Chen, *Mater. Horiz.* **2021**, *8*, 351.
[15] X. Zhao, F. Chen, Y. Li, H. Lu, N. Zhang, M. Ma, *Nat. Commun.* **2018**, *9*, 3579.
[16] J. Lu, J. Gu, O. Hu, Y. Fu, D. Ye, X. Zhang, Y. Zheng, L. Hou, H. Liu, X. Jiang, *J. Mater. Chem. A* **2021**, *9*, 18406.
[17] H. Liu, X. Wang, Y. Cao, Y. Yang, Y. Yang, Y. Gao, Z. Ma, J. Wang, W. Wang, D. Wu, *ACS Appl. Mater. Interfaces* **2020**, *12*, 25334.
[18] Y. Zhao, N. Yang, X. Chu, F. Sun, M. U. Ali, Y. Zhang, B. Yang, Y. Cai, M. Liu, N. Gasparini, J. Zheng, C. Zhang, C. Guo, H. Meng, *Adv. Mater.* **2023**, *n/a*, 2211617.
[19] Y. Shi, R. Wang, S. Bi, M. Yang, L. Liu, Z. Niu, *Adv. Funct. Mater.* **2023**, *n/a*, 2214546.
[20] L. Hu, P. L. Chee, S. Sugiarto, Y. Yu, C. Shi, R. Yan, Z. Yao, X. Shi, J. Zhi, D. Kai, H. D. Yu, W. Huang, *Adv. Mater.* **2022**, *35*, 2205326.
[21] C. Ma, F. Xie, L. Wei, C. Zheng, X. Liu, L. Wang, P. Liu, *ACS Sustainable Chem. Eng.* **2022**, *10*, 6724.
[22] S. Wang, Y. Chen, Y. Sun, Y. Qin, H. Zhang, X. Yu, Y. Liu, *Commun. Mater.* **2022**, *3*, 2.
[23] W. Liu, R. Xie, J. Zhu, J. Wu, J. Hui, X. Zheng, F. Huo, D. Fan, *npj Flexible Electron.* **2022**, *6*, 68.
[24] Y. Cai, J. Shen, C. W. Yang, Y. Wan, H. L. Tang, A. A. Aljarb, C. Chen, J. H. Fu, X. Wei, K. W. Huang, Y. Han, S. J. Jonas, X. Dong, V. Tung, *Sci. Adv.* **2020**, *6*, eabb5367.
[25] L. Dong, M. Wang, J. Wu, C. Zhu, J. Shi, H. Morikawa, *ACS Appl. Mater. Interfaces* **2022**, *14*, 9126.
[26] S. Lin, H. Yuk, T. Zhang, G. A. Parada, H. Koo, C. Yu, X. Zhao, *Adv. Mater.* **2016**, *28*, 4497.
[27] Y. Lu, X. Qu, W. Zhao, Y. Ren, W. Si, W. Wang, Q. Wang, W. Huang, X. Dong, *Research* **2020**, 2020.
[28] W. Yuan, X. Qu, Y. Lu, W. Zhao, Y. Ren, Q. Wang, W. Wang, X. Dong, *Chin. Chem. Lett.* **2021**, *32*, 2021.
[29] Y. Feng, S. Wang, Y. Li, W. Ma, G. Zhang, M. Yang, H. Li, Y. Yang, Y. Long, *Adv. Funct. Mater.* **2023**, *n/a*, 2211027.
[30] R. Eelkema, A. Pich, *Adv. Mater.* **2020**, *32*, 1906012.
[31] E. Larrañeta, S. Stewart, M. Ervine, R. Al-Kasasbeh, R. F. Donnelly, *J Funct Biomater* **2018**, *9*, 13.
[32] N. L. Smith, A. E. Coukouma, D. C. Wilson, B. Ho, V. Gray, S. A. Asher, *ACS Appl. Mater. Interfaces* **2020**, *12*, 238.
[33] Y. Feng, J. Yu, D. Sun, W. Ren, C. Shao, R. Sun, *Chem. Eng. J.* **2022**, *433*, 133202.
[34] C. Yang, Z. Suo, *Nat. Rev. Mater.* **2018**, *3*, 125.
[35] J. Wu, Z. Wu, X. Lu, S. Han, B. R. Yang, X. Gui, K. Tao, J. Miao, C. Liu, *ACS Appl. Mater. Interfaces* **2019**, *11*, 9405.
[36] H. Zhang, W. Niu, S. Zhang, *ACS Appl. Mater. Interfaces* **2018**, *10*, 32640.
[37] Z. He, W. Yuan, *ACS Appl. Mater. Interfaces* **2021**, *13*, 1474.
[38] W. Qiu, C. Zhang, G. Chen, H. Zhu, Q. Zhang, S. Zhu, *ACS Appl. Mater. Interfaces* **2021**, *13*, 26490.
[39] Y. Jian, B. Wu, X. Le, Y. Liang, Y. Zhang, D. Zhang, L. Zhang, W. Lu, J. Zhang, T. Chen, *Research* **2019**, 2019.
[40] Y. Zhang, Y. Zhao, Z. Peng, B. Yao, Y. Alsaid, M. Hua, D. Wu, Y. Qiu, Q. Pei, X. Zhu, Z. He, X. He, *ACS Mater. Lett.* **2021**, *3*, 1477.
[41] Y. Wei, L. Xiang, P. Zhu, Y. Qian, B. Zhao, G. Chen, *Chem. Mater.* **2021**, *33*, 8623.
[42] L. Zhu, J. Xu, J. Song, M. Qin, S. Gu, W. Sun, Z. You, *Sci. China Mater.* **2022**, *65*, 2207.
[43] B. Zheng, H. Zhou, Z. Wang, Y. Gao, G. Zhao, H. Zhang, X. Jin, H. Liu, Z. Qin, W. Chen, A. Ma, W. Zhao, Y. Wu, *Adv. Funct. Mater.* **2023**, *n/a*, 2213501.
[44] D. Sun, Y. Feng, S. Sun, J. Yu, S. Jia, C. Dang, X. Hao, J. Yang, W. Ren, R. Sun, C. Shao, F. Peng, *Adv. Funct. Mater.* **2022**, *32*, 2201335.
[45] Y. Feng, J. Yu, D. Sun, C. Dang, W. Ren, C. Shao, R. Sun, *Nano Energy* **2022**, *98*, 107284.

© 2023 Wiley-VCH GmbH

16163028, 0, Downloaded from https://onlinelibrary.wiley.com/doi/10.1002/adfm.202304625 by Georgia Institute Of Technology, Wiley Online Library on [06/08/2023]. See the Terms and Conditions (https://onlinelibrary.wiley.com/terms-and-conditions) on Wiley Online Library for rules of use; OA articles are governed by the applicable Creative Commons License